ChemComm
Chemical Communications

ChemComm

View Article Online
DOI: 10.1039/D6CC01757F

COMMUNICATION

From RRDE to GDE: Loading-Dependent H_2O_2 Selectivity Loss in Sn- and Sb-N-C Catalysts

Marco Mazzucato,[a] Riccardo Marinello,[a] and Christian Durante*[a]

Received 00th January 20xx,
Accepted 00th January 20xx

DOI: 10.1039/x0xx00000x

Electrochemical H_2O_2 synthesis offers a sustainable route to advanced oxidation processes. Using Sn- and Sb-containing single-site catalysts, we reveal a strong effect of catalyst loading: the RRDE selectivity is lost at gas diffusion electrodes with higher loadings. These results highlight the need for caution when transposing model measurements to device-relevant conditions.

The use of water as a hydrogen source for the synthesis of useful chemicals is of growing interest,[1] particularly in processes where H_2 comes from steam reforming. Electrochemical oxygen reduction reaction (ORR) via a 2 electron pathway (2e-ORR) offers an interesting alternative to the consolidated anthraquinone process, by simultaneously eliminating the needed of gaseous hydrogen, organic solvents, and allowing a more decentralized production.[2,3] The development of efficient and selective electrocatalysts is the first crucial step for enabling the practical implementation of this approach. In particular, catalysts capable of promoting the 2e-ORR pathway toward H_2O_2 while suppressing the competing four-electron reduction to water are highly desirable.[3,4] Historically promising catalysts for H_2O_2 were based on Pd, Au, and Hg, with all the related problems (cost, availability, and safety), but the recent interest is to move to cheaper metal-based catalysts and metal-free catalysts.[3,5] For this reason, a reliable evaluation of catalytic activity and selectivity is essential during the early stages of catalyst development. Electrochemical screening methods at the laboratory scale play a key role in identifying promising materials and understanding their intrinsic behavior under controlled conditions; in other words, they cannot forbear quick evaluation of the activity and selectivity of the electrocatalysts. For this reason, testing in a rotating ring disk electrode (RRDE) is a well-consolidated practice to simultaneously probe the ability to reduce O_2 (activity) and the effectiveness of following the desired pathway (selectivity). This setup is highly versatile across a wide pH range and in several electrolytes,[6–8] thanks to the possibility of preparing thin films on a glassy carbon (GC) electrode, which exhibits good chemical and electrochemical inertness under these conditions. If on the one hand, this setup allows a fast screening, on the other, it is generally not representative of a practical device where a gas diffusion electrode (GDE) permit of overcome the problem of O_2 low solubility in water. One of the main issues and a not well-documented aspect is the role of “support” in the electrochemical screening experiment. If GC is known to have a low interference in RRDE measurements since it is generally well covered with a catalyst layer, in the GDE experiment, the intrinsic porosity of carbon paper or carbon cloth used for supporting the catalysts makes the exposure of itself not negligible. This is more evident going to neutral or alkaline media, in particular when catalyst loading is low (ca. 10^{-1} mg cm^{-2}); this is caused by shifting to an outer sphere electron transfer mechanism, which makes the metal role less central, in favour of the carbon matrix itself.[9] For these reasons, this work places particular emphasis on the effect of catalyst loading in GDE measurements, to show how selectivity can be easily lost as the catalyst loading increases. For this scope, we prepare two different catalysts featuring *p*-block metals, namely Sn (Sn-N-C) and Sb (Sb-N-C), with similar activity and different selectivity to show the loading-dependent H_2O_2 selectivity loss, in particular in the GDE setup. The use of Sn and Sb was chosen not only to study unconventional metal centers,[10] but also to avoid the heterogeneous Fenton reaction, which is not reported for these metal centers.[11] The effectiveness of single-atom catalysts based on Sn has been shown computationally,[12] and practically, claiming both two[13–15] and four[16–18] electrons for ORR pathways. As Sn, Sb is a low-toxic, stable, and relatively abundant resource. Sb’s electron-rich nature provides a strong affinity for electron-deficient O_2 molecules, facilitating simple chemical reactions and electron transfer.[10] Also, in this case, there are several examples of Sb-based single-atom catalysts. For example, Wang et al. developed a p-block single-atom Sb catalyst featuring an Sb-N_4 coordination environment.[10,19]

a. University of Padova, Department of Chemical Science, Via Marzolo 1, Padova, 35131, Italy

View Article Online
DOI: 10.1039/D6CC01757F

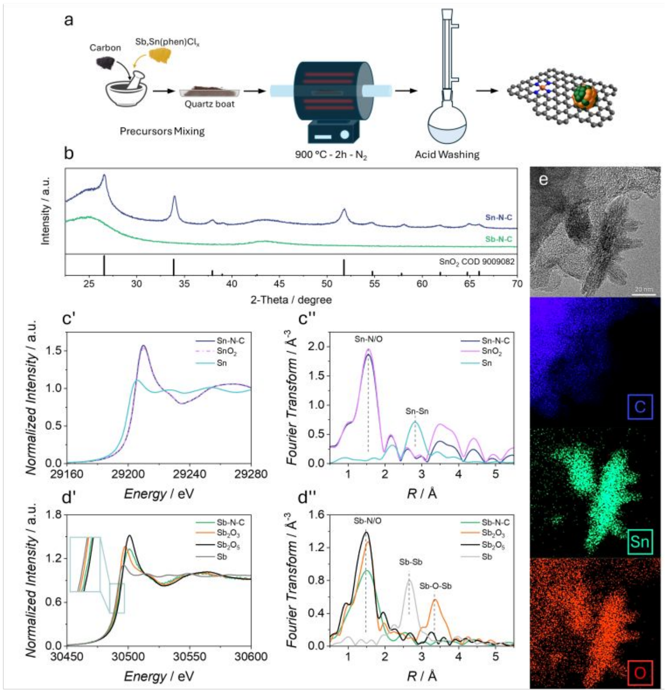

Fig. 1 a) schematic view of the synthetic pathway. b) XRD profile for the two catalysts is reported with the SnO_2 phase reference reported for Sn-N-C. c') XANES region of Sn-N-C catalysts with Sn^0 and Sn^{4+} references, c'') reports the Fourier transform of the EXAFS region. d') XANES region of Sb-N-C catalysts with Sb^0, Sb^{3+}, and Sb^{5+} references, d'') Fourier transform of the EXAFS region. e) the STEM-EDX image for the Sn-N-C is reported.

Their study revealed that the *p* orbitals of Sb can efficiently interact with the *p* orbitals of oxygen, providing adequate adsorption strength for oxygen intermediates while reducing the reaction energy barrier. Also, for the case of Sb, both four[20–22] and two[23,24] electrons catalysts have been reported. Here, Sn- and Sb-N-C catalysts were prepared with a two-step procedure as reported in **Fig. 1**a. The first step is a pyrolysis of a mixture of metal-phenanthroline complex and commercial Vulcan XC72 carbon black. This was done in an inert atmosphere (N_2) at 900 °C for 2h. After this, the obtained powder was leached in in 1 M H_2SO_4 for 3h at 100°C. This produces, in principle, a clean N-doped graphitic matrix with dispersion of single-site atoms (see SI for details); instead, Sn and Sb had two different behaviours. Sn is known from previous studies[15] to form metallic Sn during the pyrolysis that is then oxidized to SnO_2 during the acid washing, as verified here (Sn-N-C 1T in **Fig. S1**). Also in this study, the presence of SnO_2 was verified via XRD (**Fig. 1**b) and via XAS (**Fig. 1**c) analysis. Indeed, this produces a catalyst, which is a mixture of SnN_x single-atom center and SnO_2, which does not catalyze H_2O_2 decomposition (details are given below). The presence of a SnN_x e was proven by intensive washing[25] and by performing XAS analysis (washed Sn-N-C 1T in **Fig.** S1), observing a decrease in the Sn-Sn signal of the oxide, as well as the disappearance of the SnO_2 signal in the XRD (**Fig. S1**a). The choice of not further making other treatments was made to simplify the synthesis, and due to promising results in similar studies in neutral media.[15] Sb, on the other hand, does not produce any metallic phase during pyrolysis (Sb-N-C 1T in **Fig. S1**), and therefore also in the final catalysts (XRD in **Fig. 1**b). More in detail, the XAS reveals that all Sn is in the 4+ state, which is both compatible with SnN_x sites and SnO_2; in particular, this is clear from the superimposition of XANES spectra in **Fig. 1**c' and by the absence of Sn-Sn signal of the metallic Sn in EXAFS profile (**Fig. 1**c''). Also, the Sn-Sn component of the oxide is lower in the catalyst, suggesting the coexistence of the two species. This is further supported by the washed Sn-N-C catalyst, which still shows a XAS signal compatible with a 4+ oxidation state, but no XRD peak of the oxide (**Fig. S1**). For Sb, the XANES signal lies between the Sb_2O_3 and Sb_2O_5 signal, corresponding to an oxidation state greater than 3+. This is in line with previous findings on Sb-N-C,[21] even if elsewhere lower oxidation states (< +3) are reported.[19,20,23] Finally, a STEM-EDX image was taken for Sn-N-C to evaluate the morphology of SnO_2. As expected from the triangular-like XRD peaks (**Fig. 1**b), nanoparticles show irregular (non-spherical) shapes as clearly evident in **Fig. 1**e, and a non-monodisperse dimensional distribution. XRD peak width suggests a crystallite dimension of around 15 nm (from Scherrer equation), which aligns with what was observed with TEM. Finally, the Fourier transform on a portion with nanoparticles (**Fig. S2**) shows spots that resemble the periodicity of SnO_2. Elemental map reveals the superimposition of Sn and O in the nanoparticle region, but at the same time, some Sn is also detected in the carbonaceous portion of the sample, corroborating the thesis on a possible SnN_x functionalization. In conclusion, both catalysts are believed to contain metal single-site centers coordinated with nitrogen, in the case of Sn, together with some SnO_2 particles.

Following the chemical and physical characterization, a first test on RRDE was performed. Each catalyst was drop-cast on a GC disk-Pt ring electrode with a loading of 0.6 mg cm^{-2}. Linear sweep voltammetry (LSV) was recorded in 0.1 M KOH (pH = 13) between 1 and −0.4 V vs. RHE with a scan rate of 5 mV s^{-1} at a rotation of 1600 rpm (**Fig. 2**a). To collect H_2O_2, practically HO_2^- at this pH, the ring potential was set to 1.5 V vs. RHE. As it is possible to observe (**Fig. 2**a), Sb sample shows a higher faradic efficiency peaking over 60 %, while Sn-N-C reaches a maximum of 35%. It is also clear that those two catalysts show a 2-step reaction, between 0.8 and 0 V vs. RHE, the LSV reaches a first plateau current, which corresponds to the region where the selectivity has a peak. Then, between 0 and −0.4 V vs. RHE, the current reaches a slightly lower (higher in modulus) value, with selectivity stabilizing at the lower observed value along all LSV. This could imply a first region where O_2 is reduced to both H_2O_2 and H_2O, and a second one where H_2O_2 is also reduced to H_2O. This behavior is common to the two catalysts. Compared to the bare glassy carbon, there is a clear difference in activity (**Fig. S3**a), proving a catalytic activity. To better understand the role of SnO_2 in Sn-N-C, measurements on the sole oxide were made. **Fig. S4**a-c shows the RRDE response. SnO_2 is revealed to be similar in activity compared to bare glassy carbon (GC) with a low production rate of H_2O_2 despite a good selectivity, higher than Sn-N-C. The selectivity drops to a lower value below 0.3 V vs. RHE. This excludes a possible effect of SnO_2 in catalysing the decomposition of H_2O_2 in the potential region where Sn-N-C and Sb-N-C show the biggest difference. This is also corroborated by a CV experiment with O_2 and H_2O_2.

DOI: 10.1039/D6CC01757E

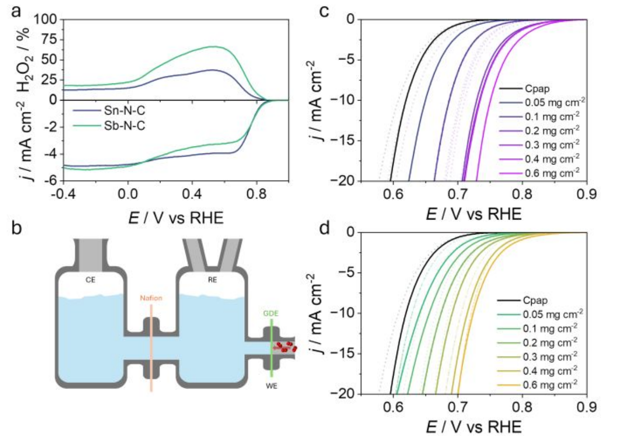

Fig. 2 a) Linear sweep voltammetry and peroxide yield of the two prepared catalysts (v = 5 mV s^{-1}, 1600 rpm, 0.1 M KOH (+ K_2SO_4 to improve conductivity), O_2-saturated; loading 0.6 mg cm^{-2}). b) GDE H-cell pictorial scheme. c, d) Linear sweep voltammetry in GDE configuration for Sn-N-C (c) and Sb-N-C (d) at different tested loading, compared to the bare carbon paper support (Cpap). Also, in this case, the cathodic compartment contains 0.1 M KOH (+K_2SO_4). In light color, dotted line, the LSV after 4h is reported.

In the presence of O_2, two distinct reduction peaks are observed (**Fig. S4**d). The peak at more negative potential is also seen with H_2O_2, which supports the idea of H_2O_2 being reduced at more negative potential compared to O_2 and/or of a variation of mechanism below 0.3 V. The next step was to move to a GDE setup to close the gap with a practical device. For this purpose, an H-cell with an aperture to place a diffusion electrode (**Fig. 2**b) was used. This consists of two 150 mL chambers filled with electrolytic solution. On the counter electrode side, an acidic solution (pH 1) was used, while on the cathodic side, an alkaline solution was placed (pH 13). This was done to help proton diffusion through the membrane by increasing the gradient. Materials were vacuum filtered on a carbon paper with a microporous carbon layer (MPL) at different loadings (all the experimental details are given in the SI). The first test was done on the very same loading used for RRDE, namely 0.6 mg cm^{-2}. The activity observed is in line with that of RRDE (**Fig. S3**b), when the current is converted to pure kinetic current using the Koutecký–Levich equation. This is a very useful comparison that allow to quickly understand if passing to a GDE causes some hindrance to the activity. Passing to the evaluation of the selectivity (faradic efficiency, FE), chronopotenziometry was performed by fixing the current at −5 mA cm^{-2} for 4 h. Every 30′ the solution was sampled for evaluating the H_2O_2 production, using the Ti(IV) complexation method (see SI for details). GDE selectivity performances are not reaching what is observed on RRDE. Indeed, for Sn-N-C, the FE for a loading of 0.6 mg cm^{-2} is around 7.5% (**Fig. 3**b), which is lower than the maximum observed with RRDE (**Fig. 2**a) and lower even if considering the same potential region (around 0.75 V) where the chronopotenziometry takes place. The same is true for Sb-N-C, which reaches a FE of 21% (**Fig. 3**d), again lower than the peak observed in RRDE (**Fig. 2**a) and in the same potential region of the chronopotenziometry. If compared with the bare carbon paper (Cpap) used for supporting the material, the activity is clearly improved for both catalysts (**Fig. 2**c and d), even if the advantage of having a catalyst layer is less marked compared to the GC (**Fig. S3**a); in other words, the carbon paper with MPL is more active than the GC. In terms of selectivity, the situation is the opposite. The bare carbon paper is revealed to be more selective than the two catalysts, reaching over 80% of FE. These relatively surprising results lay the basis for studying the effect of loading on GDE. The idea was to understand if there is a balance between activity (lower overpotential) and selectivity. **Fig. 2**c and **Fig. 2**d show the variation of LSV as a function of the loading. For Sn-N-C (**Fig. 2**c), there is an initial important shift toward more positive potential for loading ≤ 0.1 mg cm^{-2}, which than flatten out between 0.2 and 0.6 mg cm^{-2}, possibly suggesting that not all material is working efficiently or that the catalysts are not ideally homogeneous. Looking at the production rate ($\dot{n}$), namely the number of moles produced per hour, it is clear that, being the current fixed, and therefore the charge, higher loading is detrimental to productivity (**Fig. 3**a). This is indeed true for selectivity that decreases with increasing loading (**Fig. 3**b). The very same behavior is observed for Sb-N-C. The LSV (**Fig. 2**d) shifts to a more positive potential, this time more "linearly" compared to Sn-N-C. Looking at the production rate ($\dot{n}$), the same trend is observed, except for 0.05 mg cm^{-2}, that reveal to be a little bit more productive (**Fig. 3**c). The discrepancy between these results and the corresponding FE is because the production rate is evaluated as a linear fit of concentration at each sampling point (every 30′), while faradic efficiency is calculated at the end of chronopotenziometry.

This decrease in selectivity can be explained by considering both the growth of the catalyst layer and the slight positive shift of the working potential. It can be said that the residence time for a diffusing species is expected to increase with the square of the layer thickness, which linearly scales with the loading. Consequently, H_2O_2 is more likely to encounter additional active sites where it can undergo further reduction, particularly at N and metallic centers. Moreover, in the GDE configuration, the absence of forced convection limits product removal, although local alkalinization can promote electrostatic repulsion between HO_2^- and OH^-, thereby facilitating peroxide diffusion.[26] Also, under galvanostatic operation, the working potential is not directly controlled. The two investigated catalysts operate at more positive potentials than the bare carbon paper, which actually works within a more favorable potential window for H_2O_2 selectivity. To support this interpretation, measurements were performed using only the carbon support (C) on both RRDE and GDE at a loading of 0.6 mg cm^{-2} (**Fig. S4**). While C exhibited a comparable H_2O_2 production rate but lower activity on RRDE, switching to the GDE configuration resulted in a production similar to that of Cpap. In this case, the behavior cannot be attributed to mass transport but to the lower working potential, beneficial for selectivity, and with the absence of highly active sites capable of further reducing H_2O_2. Discussing the RRDE/GDE discrepancy, the next step was to understand the feasibility of H_2O_2 production with the catalyst used. An energy consumption (electrochemical work, W_{el}) parameter was defined as a function of the overpotential, current, and the production rate, which is also connected to FE (see SI, S2.7). This gives a work normalized by

View Article Online
DOI: 10.1039/D6CC01757F

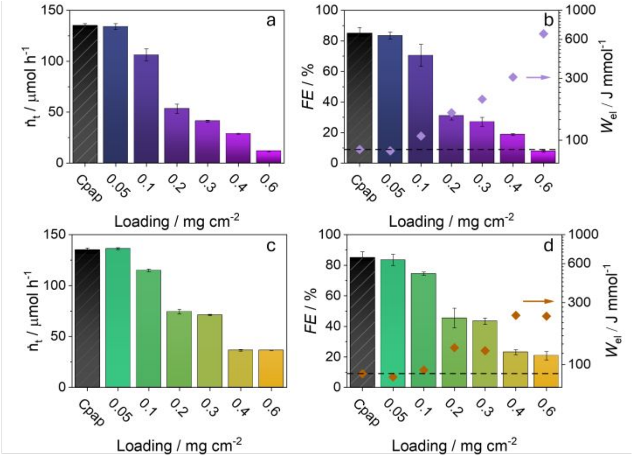

Fig. 3 Rate production of H_2O_2 for a) Sn-N-C and c) Sb-N-C evaluated as the slope of the linear fit between the produced amount at each sampling step, plotted against the catalyst's loading. b, d) The Faradic efficiency is plotted against the loading and reported together with the energy consumption for b) Sn-N-C and d) Sb-N-C.

the moles produced, whose magnitude is inversely proportional to the efficiency; lower values are given by the best combination of activity and selectivity. Dots in secondary axes of **Fig. 3**c, d report the obtained value for all the loadings and Cpap. It reaches an energy consumption of 85 J $mmol^{-1}$, which is slightly higher than that of the two catalysts at 0.05 mg cm^{-2}. For Sn-N-C, the value is 83, while for Sb-N-C is 80 J $mmol^{-1}$, which represents an improvement of around 6% compared to Cpap. Passing to a loading of 0.1 mg cm^{-2} results in a not competitive value for Sn-N-C (109 J $mmol^{-1}$), while Sb-N-C is still close to bare carbon paper performance (91 J $mmol^{-1}$). These results align with the better selectivity observed for Sb-N-C in RRDE, but far from the expected value of H_2O_2 production. This is extremely evident at 0.6 mg cm^{-2}, where the W_{el} reach 660 J $mmol^{-1}$ for Sn-N-C and 236 J $mmol^{-1}$ for Sb-N-C. These results clearly show how important it is to carefully separate the activity and the selectivity when a GDE is used, since trapping phenomena are amplified due to the absence of forced mixing in the proximity of the electrode, as is true for RRDE. Also, fixing a current could cause a shift in potential and FE with loading affecting the work consumption.

In summary, two *p*-block metal catalysts were prepared to produce H_2O_2 in alkaline media via a 2e-ORR. Catalyst loading played a pivotal role in performance; specifically, increased loading enhanced activity at the expense of selectivity. While bare carbon paper exhibited the highest intrinsic selectivity, energy consumption analysis suggests that low catalyst loadings (< 0.1 mg cm^{-2}) can improve activity without compromising the selectivity. This can be explained by the fact that a tiny amount can lower the reaction overpotential without providing enough active sites to further reduce the produced H_2O_2. These findings underscore the necessity of optimizing both support and loading in GDE systems, since mass transport and forced convection differ significantly from RRDE setups. It also highlights the value of parameters like energy consumption and Koutecký–Levich analysis for balancing voltage efficiency and selectivity, and comparing RRDE and GDE measurements more easily.

Acknowledgments

MIUR is acknowledged for the support to the project financed by the European Union - Next Generation EU - Bando PRIN 2022 PNRR – M4.C2.1.1: Progetto: P2022WANKS - ECHO-EF. Experiments were performed on the SAMBA beamline (using the Chemistry support lab) at SOLEIL Synchrotron, France (proposal numbers 20220248 & 20240787). We are grateful to Andrea Zitolo for assistance and to the SOLEIL staff for smoothly running the facility.

Conflicts of interest

There are no conflicts to declare.

Data availability

The data supporting this article are included in the supplementary information (SI). Supplementary information is available. See DOI:

Notes and references

1. Kundu, B.K. et al. (2024). *Chem. Sci.*, 15, 16424–16435
2. Wen, Y. et al. (2022). *Angewandte Chemie*, 134, e202205972
3. Yang, S. et al. (2018). *ACS Catal.*, 8, 4064–4081
4. Verdaguer-Casadevall, A. et al. (2014). *Nano Lett.*, 14, 1603–1608
5. Mazzucato, M. et al. (2024). *ACS Catal.*, 14, 6369–6403
6. Zuccante, G. et al. (2025). *Mater Renew Sustain Energy*, 14, 58
7. Okazaki, T. et al. (2024). *ACS Sustainable Chem. Eng.*, 12, 9856–9863
8. Rojas-Carbonell, S. et al. (2018). *ACS Catal.*, 8, 3041–3053
9. Ramaswamy, N. et al. (2011). *J. Phys. Chem. C*, 115, 18015–18026
10. Liang, H. et al. (2025). *Advanced Materials*, 37, e10356
11. Liu, Y. et al. (2023). *Chemical Engineering Journal*, 466, 143147
12. Zhang, Y. et al. (2023). *Molecules*, 28, 5571
13. Gu, Y. et al. (2025). *Nat. Synth*, 4, 614–621
14. Xu, P. et al. (2026). *Angew Chem Int Ed*, 65, e23314
15. Zhao, L. et al. (2025). *ChemSusChem*, 18, e202401758
16. Fu, X. et al. (2026). *Small*, 22, e13912
17. Lin, X. et al. (2024). *Advanced Energy Materials*, 14, 2303740
18. Wang, X. et al. (2024). *J. Am. Chem. Soc.*, 146, 21357–21366
19. Wang, T. et al. (2021). *Angew Chem Int Ed*, 60, 21237–21241
20. Gu, Y. et al. (2022). *Angewandte Chemie*, 134, e202202200
21. Zhang, D. et al. (2022). *Chemical Engineering Journal*, 439, 135700
22. Zhang, Y. et al. (2024). *Nano Lett.*, 24, 4291–4299
23. Yan, M. et al. (2024). *Advanced Materials*, 36, 2402963
24. Yan, M. et al. (2023). *Nat Commun*, 14, 368
25. Mazzucato, M. et al. (2022). *ACS Appl. Mater. Interfaces*, 14, 54635–54648
26. Cui, L. et al. (2024). *Nat Commun*, 15, 10632

View Article Online
DOI: 10.1039/D6CC01757F

Data availability

The data supporting this article are included in the supplementary information (SI). Supplementary information is available. See DOI: